Practical Considerations of Wideband Radar Waveforms

Rich Simeon
EECS 725, Spring 2017

Abstract

It is well-known that radar transmission bandwidth plays a key role in radar measurement accuracy and resolution. Different methods for modulating the wideband radar signal all have advantages and disadvantages with respect to various theoretical (e.g. Doppler sensitivity, target resolution) and practical (e.g. power amplifier linearity, design complexity, spectral distortion) considerations.

This project will first give an overview of popular wideband radar waveforms (LFM, binary codes, and polyphase codes), and their advantages and disadvantages with respect to various measures of goodness such as autocorrelation mainlobe width, sidelobe levels, spectral containment, and ambiguity function for Doppler sensitivity. It will then simulate the chirp waveform (LFM), considered a fundamental wideband waveform, against a P4 (polyphase) code sequence, and the measures of goodness will be compared. Finally, example targets will be simulated to show how the two waveforms compare in different Doppler scenarios and target separation.

Introduction

The term Waveform Diversity is partially defined by IEEE as the “optimization of the radar waveform to maximize performance according to particular scenarios and tasks” [1]. It continues to mention that other domains such as time, frequency, coding, and polarization may be explored. This project paper concentrates on the make-up of the transmitted radar waveform pulse, and in particular is focused on exploring the advantages and disadvantages of the different classes of radar waveforms with respect to performance as well as practical factors such as ease of implementation.

An overview of the current types of radar waveforms is presented, along with the motivations for developing the different types of waveforms. Measures of goodness are then listed, in order to facilitate comparisons of the different types. Research findings from literature are then presented. Simulation of two waveforms is performed to illustrate the waveform strengths and weaknesses via scenarios. Finally, we conclude the paper with use cases where the different waveforms could be of practical use.

Motivation

Towards the end of World War II, peak transmit power was limited by the current amplification technology of the time, namely microwave transmission tubes [2] (recall that the transistor would not be invented until 1947). Radar waveforms were purely continuous-wave (CW) pulses with high-power transmission for long range and short-duration for better range resolution. Subsequent research into radar pulse compression revealed the now familiar expression of range resolution, $\Delta r = \frac{c}{2B}$, wherein the key takeaway from pulse compression is that bandwidth, not pulse duration, is the key determinant in range resolution. Furthermore, advances in waveform generation technology via digitization has opened the possibility for sophisticated waveforms other than CW that can achieve better resolution using lower power. In this paper, we discuss these “sophisticated” waveforms and their merits as well as shortcomings.

Measures of Goodness

Before exploring the different waveform types, we begin by listing the key characteristics of radar waveforms that determine their utility and uniqueness.

Radar echoes are typically detected via matched-filtering, where a copy of the transmitted waveform signal is cross-correlated with the incoming receive signal (usually at baseband, after one or more rounds of down-conversion). The output of the matched filter is examined to determine if there are any strong correlation peaks that are indicative of a target-of-interest. As such, two key measures of goodness from matched filtering are the mainlobe width and sidelobe levels from the autocorrelation of the waveform.

The mainlobe width is typically measured in terms of t/τ (τ being the pulse length), a normalization step that allows for comparisons with other waveforms. A small width allows for better range resolution, since the exact time that the echo is received can be determined with more certainty. It also accommodates detection of closely-spaced targets.

The sidelobe level is typically measured as a factor of mainlobe power in dB. Low sidelobe levels allows for the detection of targets that may be close together in space but may have much different radar cross sections (RCS). High sidelobe levels from a strong RCS target may mask a close-by target with a weak RCS (see Figure 1).

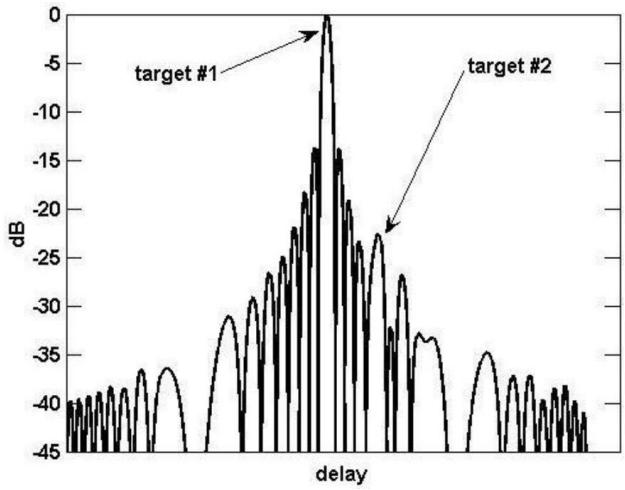

Figure 1-Target 2 masked by sidelobes of Target 1 [Blunt, 3]

While the two aforementioned characteristics are mostly theoretical measurements, the AM envelope of the waveform is important with respect to practical transmission of the waveforms. Due to the nature of linear power amplifiers (PA), signals with constant or near-constant envelopes can remain close to the power amplification limits of the PA without entering the non-linear region of the amplifier (e.g. clipping). Conversely, signals with high peak-to-average ratios (PAR, or “crest factor”) must lower their average power so that the signal peaks do not transfer into the non-linear or clipping region of the amplifier. Figure 2 below shows the effects of

autocorrelation with and without clipping due to saturation. Peak sidelobe levels degrade by 14.7dB due to clipping as a result of the intermodulation products that result from operating in the amplifier's non-linear region [4].

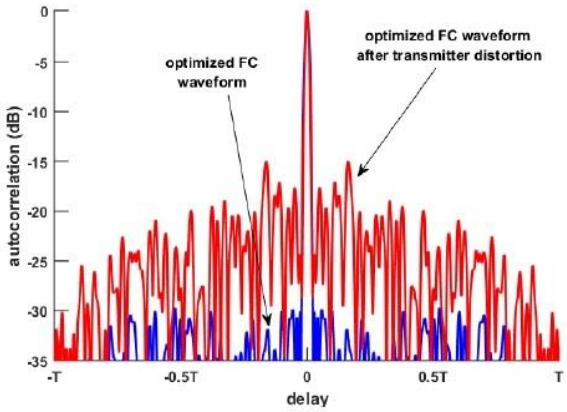

Figure 2- Effects of transmit saturation on autocorrelation sequence [Blunt, 4]

Spectral containment is also of practical importance. While waveforms can be constrained within a certain bandwidth, usually the waveform will have some spectral leakage outside the designated bandwidth, which may be truncated by the transmitter's driver amplifiers. The resulting distortion from the bandlimiting may result in range-straddling (cusping) losses on the received signal, which would affect range accuracy [5]. Windowing can help, but at the cost of increased mainlobe width.

Finally, the ambiguity function is a useful measure of waveform effectiveness in the presence of Doppler shifts (as is typical of moving targets). This function is essentially the cross-correlation of a transmitted signal and its frequency-shifted version, and is defined as:

$$\chi(\tau, f_D) = \int_{-\infty}^{\infty} s(t)s^*(t-\tau)e^{-j2\pi f_D t}dt$$

As will be shown later, some waveforms perform poorly when correlating to a Doppler-shifted echo. An example of an ambiguity function for a rectangular pulse is shown below in Figure 3 [3]. Plots generally are shown as contour plots, with the z-axis being the absolute value of the ambiguity function, and x-axis and y-axis being autocorrelation lag and Doppler frequency shift, respectively. In the case of the rectangular pulse ambiguity plot, an important observation here is the severe drop in correlation as Doppler frequency (e.g. target closing speed) increases. Essentially, a target can disappear if moving fast enough relative to the radar platform.

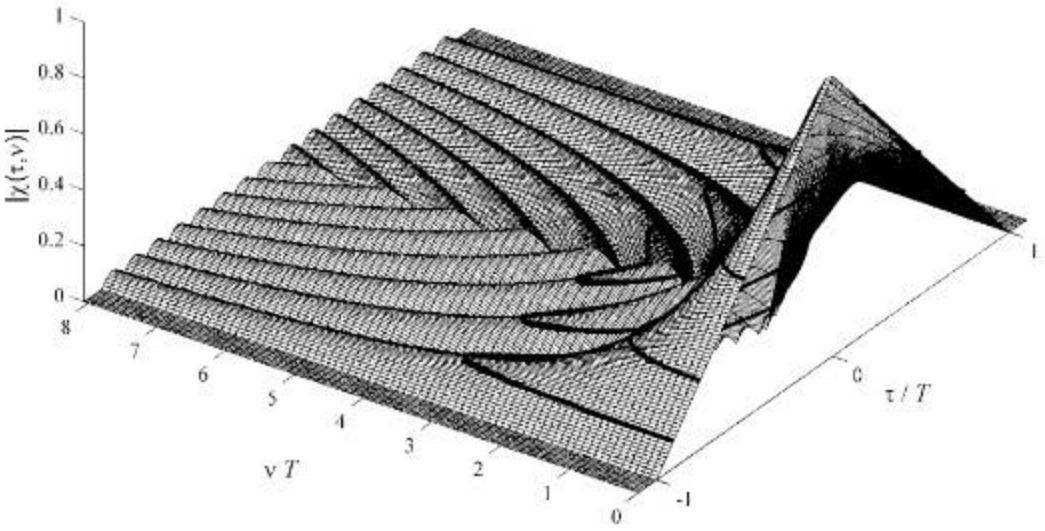

Figure 3- Ambiguity function of a continuous wave rectangular pulse [3]

Research findings

The major classes of waveforms can be distilled into the basic CW rectangular pulse, FM waveforms, phase codes, frequency codes, and random noise waveforms [4]. Of particular interest in the paper are the FM and phase codes, since these are two of the more popular waveforms used for radar.

Linear Frequency Modulation (LFM) – also known as the chirp pulse, this form of FM was one of the earliest wideband waveforms. The expression for the chirp pulse is:

$$\theta(i) = \pi kiTt^2$$

where k is the chirp rate and T is the sample period. Generation of the pulse is easy to implement (surface acoustic waves, VCXO) and easy to detect (stretch processing). The continuous phase characteristics results in the envelope of LFM having a constant modulus, thus maintaining a low PAR, and is conducive to operating in the high amplification region of power amplifiers. Peak sidelobe levels are 13dB below the mainlobe, which is not necessarily ideal; while windowing can lower the sidelobe levels, it comes at a cost of widening the mainlobe.

Binary Codes – These codes were the earliest form of phase codes using pseudo-random zero-autocorrelation codes, and are called binary codes because the phases of the chips (or bits) are either 0 or 180 degrees (essentially -1 or +1). The most common sequence of binary codes are

Barker codes, which have the unique property of having sidelobes levels of $1/N_c$ of the mainlobe level, where N_c is the code length [8]. Thus, even a modest code length can outperform the chirp pulse while maintaining the same mainlobe width. The range resolution for binary codes is equal to the reciprocal of the chip rate. A disadvantage of the binary codes is the presence of extreme phase shifts associated with binary phase shift keying, resulting in a spectrum with a sin(x)/x shape (bad spectral containment), the existence of only short code sequences (the longest known one being 13 chips long), and degraded autocorrelation properties when the return echo signal is subjected to a frequency shift (Doppler) [6]. Because of the disadvantages, and the existence of better PSK-type modulations such as polyphase codes, binary codes are not heavily used.

Polyphase Codes – Similar to binary codes, polyphase codes are a form of phase-shift keying, wherein each chip can be assigned any phase (as opposed to restricting to 0 or 180 degrees). Because of the increased degrees of freedom, these codes are generally better than binary codes since they can be designed with longer sequences [6]. Popular polyphase codes include the Frank codes, P1, P2, P3, and P4 codes, all of which generally mimic the chirp pulse as a step approximation. Because of the similarity to the chirp pulse, these polyphase codes are more tolerant to Doppler shift (termed “Doppler-tolerant” or “Doppler-resilient”). They still exhibit large phase changes, which manifests itself in the wider spectral shape and higher PAR.

Table 1 - Comparison of popular radar waveforms

	LFM	**Binary**	**Polyphase**
Mainlobe width	*Same*	*Same*	*Same*
Sidelobe suppression	*13dB below mainlobe*	*1/Nc below mainlobe*	*Best (suppression varies)*
Spectral shape	*Well-contained*	*sin(x)/x*	*sin(x)/x*
Envelope	*Constant*	*High PAR*	*High PAR*
Doppler resistance	*Very good*	*Poor*	*Good*

Simulation and Analysis

To demonstrate the effects of sidelobe interference and Doppler resilience, a MATLAB program was developed to simulate the transmission of an LFM pulse and a P4 pulse.

The power spectral density (PSD) plots of both waveforms were generated for a bandwidth of 150 Mhz at a center frequency of 200 Mhz to demonstrate the spectral leakage of the waveforms. Figure 4 below shows the results.

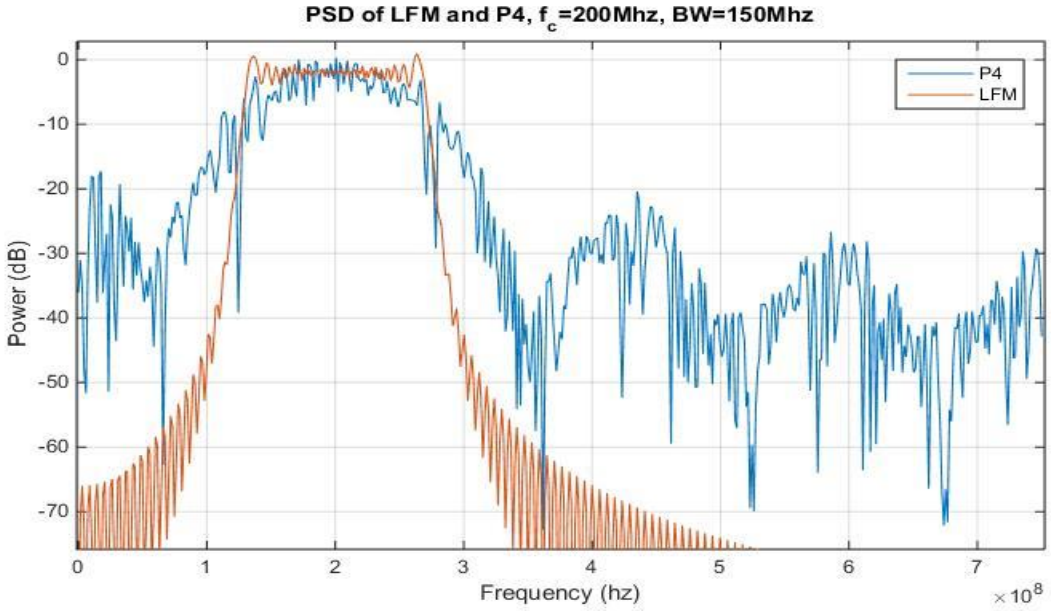

Figure 4- PSD of LFM and P4 transmissions

As seen in the figure, the spectrum for the LFM pulse is well-contained, with sharp roll-offs at the band-edges (125 Mhz and 275 Mhz). Conversely, the P4 pulse, due to the instantaneous phase change of phase-shift modulation, exhibits a sin(x)/x shape with 3dB roll-off at the band-edges [5]. For transmit filters and amplifiers with narrow bandpass characteristics, this can distort the actual transmitted waveform as described earlier and subsequently destroy the good sidelobe rejection characteristics in the waveform design. While the simulation did not perform any windowing on the chips, it is possible to apply various pulse shapes besides the rectangular pulse used in order to lower the sidelobe levels.

Next, the autocorrelation sequences for both waveforms are compared. Figure 5 shows an overlaid autocorrelation sequence of both LFM and P4 waveforms for a pulse compression ratio

(PCR) of 64, and five samples per chip. The amplitude is plotted logarithmically to emphasize the sidelobe levels for each waveform. The mainlobe width is the same for both waveforms (as expected, since the P4 waveform is derived from the LFM waveform). However, the noticeable difference between the two waveforms is in the sidelobe levels immediately surrounding the mainlobe. The P4 waveform is clearly superior in terms of sidelobe rejection, with the first sidelobe 30dB below that of the mainlobe, as compared to the first sidelobe of the LFM waveform at 14dB below the mainlobe. Out at farther lags (starting at the fourth sidelobe), the sidelobe levels are comparable. The low rejection of sidelobes around the mainlobe is ideal for distinguishing closely-separated targets; high sidelobe levels would mask a low-RCS target within the high sidelobes of a high-RCS target as shown back in Figure 1.

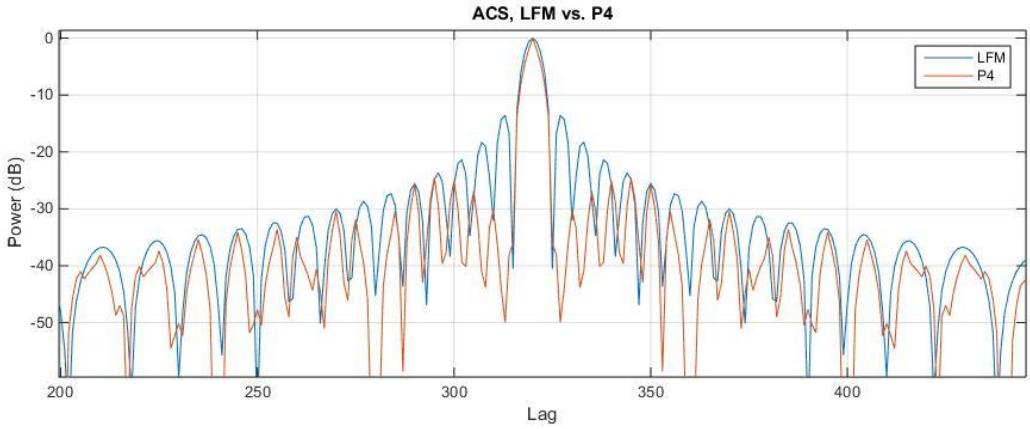

Figure 5 - Autocorrelation sequence comparison for LFM and P4 waveforms

Next, the P4 phase sequence is shown for a PCR of 64 to show the discrete nature of the phases. The P4 sequence is defined as:

$$\theta(i) = \left[\frac{\pi(i-1)^2}{N_c}\right] - \pi(i-1)$$

In this simulation, four samples are generated per chip, so the digital output stays at a particular phase for four samples before moving on to the next chip (phase). Figure 6 illustrates that the phase sequence is smooth, similar to that of a chirp, and in fact can be interpreted as sweeping across the frequencies from high to low (negative slope in phase transitions), then back to high. The second derivative of the phase sequence is constant, meaning that the FM signal sweeps across frequencies at a constant rate.

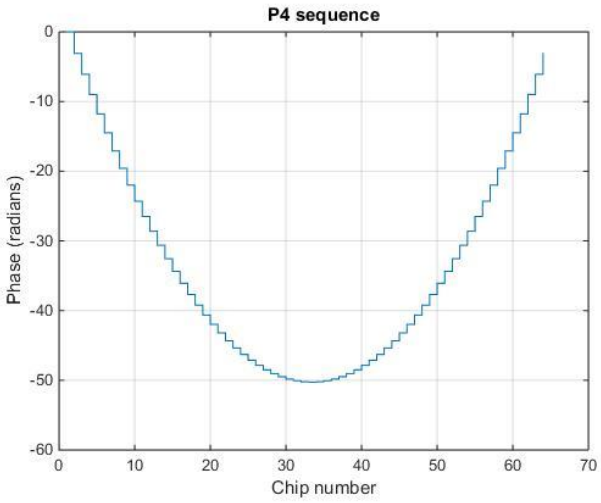

Figure 6- Discrete phases of a P4 sequence of length 64

The ambiguity function for P4 and LFM are generated as shown in the next two figures. It is customary to show the autocorrelation lag in units of t/τ to normalize the lag in terms of pulse width, and to normalize the Doppler frequency shift in units of $f_D\tau$, again to normalize the frequency shift in terms of the pulse width. In this fashion, no knowledge of carrier frequency, bandwidth, etc. is necessary to compare ambiguity functions.

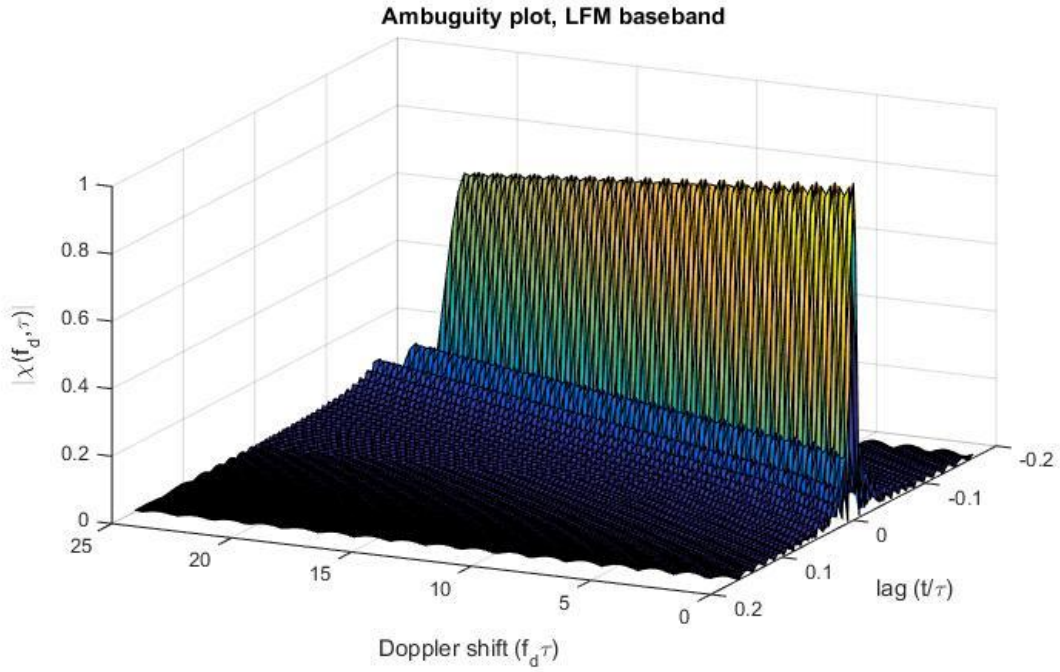

Figure 7 - Ambiguity function for an LFM waveform

The chirp waveform in Figure 7 gradually delays its mainlobe as Doppler increases. Intuitively, this makes sense, since the nature of the chirp waveform (increasing frequency as a function of

time) means that an increase in frequency of the echo appears as a delay in time. Furthermore, the mainlobe level decreases slowly out as extreme Doppler shifts.

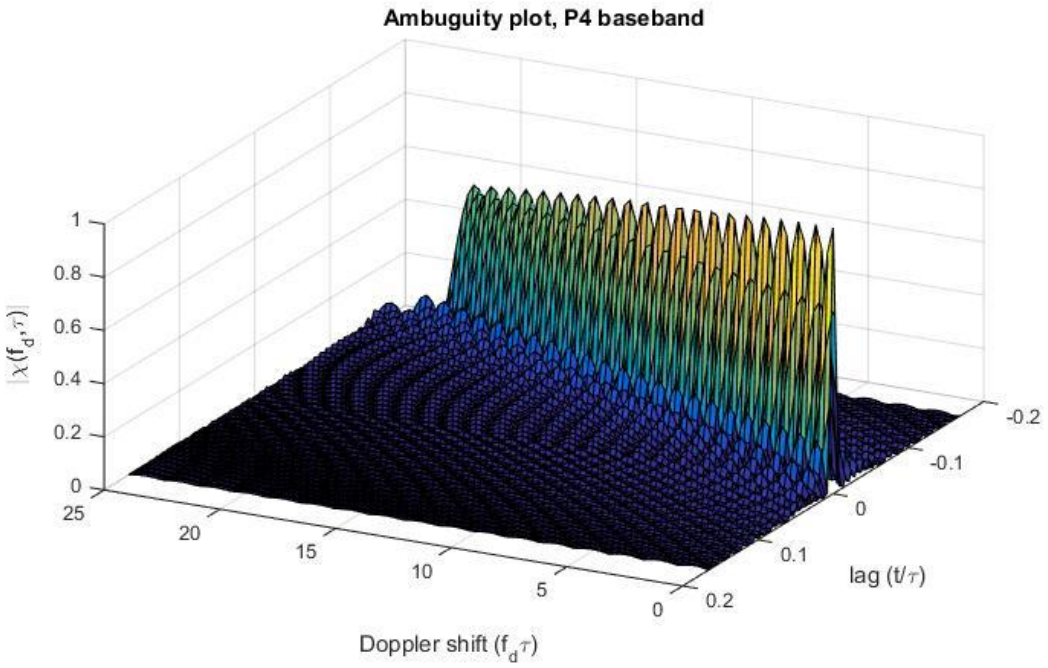

Figure 8 - Ambiguity function for the P4 waveform

The P4 waveform in Figure 8 also gradually delays its mainlobe as Doppler increases; again, the similarity of the P4 waveform to the LFM waveform should also expect this behavior. However, deep nulls in the mainlobe appear as Doppler shift increases. These nulls appear at roughly multiples of 0.5 $f_D\tau$. Fortunately, these nulls appear at very high velocities (as will be seen in the scenario simulation later in this paper). Because of the high speeds needed to encounter the first null, the P4 waveform is considered a "Doppler-resilient" waveform [6].

Two scenarios were simulated to illustrate the differences of the two waveforms (LFM and P4), particularly in the matched-filter output. Three targets are simulated at various distances, radar cross sections (RCS, equivalently represented as relative amplitudes), and closing velocities.

	Description	Target Amplitudes	Target Distances (m)	Target Velocities (m/s)
Scenario 1	Stationary targets	0.1, 1.0, 0.25	30, 90, 94	0, 0, 0
Scenario 2	Stationary and moving targets	0.1, 1.0, 0.25	30, 90, 94	4412, 0, 4412

Target 2 (the highest RCS target) is purposely stationary to keep the mainlobe and sidelobe levels and positions intact. Target 3 is placed close to target 2 and purposely assigned a low-RCS amplitude, in order to illustrate the effects of sidelobe masking.

Note that the target velocities in scenario 2 are extreme and not realistic in practice. These velocities were chosen to purposely fall into the first mainlobe null in the P4 ambiguity function, assuming X-band operation (~10 Ghz), so that the effect of Doppler can be seen in side-by-side targets.

System parameters were a bandwidth of 75 Mhz and time-bandwidth product of 128 (designated N_c). The time-bandwidth product is commonly referred to as the pulse compression ratio (PCR). A carrier frequency of 10 Ghz is used to emulate operation of an X-band radar system. Simulation parameters are four samples per chip. For the purposes of comparison, no system noise is introduced; the effects of Doppler and positioning on both waveforms can still be shown without loss of generality.

Derived parameters are presented as follows:

$$B = 75Mhz$$

$$N_c = 128$$

$$f_c = 10Ghz$$

$$\Delta r = \frac{c}{2B} = \frac{3x10^8}{2x75x10^6} = 2.0m$$

$$\tau = \frac{N_c}{B} = 1.71\mu s$$

$$t_B = \frac{1}{B} = 13.3ns$$

Figure 9 shows the LFM simulation results for both scenarios, to show the before-and-after effects of target velocity on targets 1 and 3.

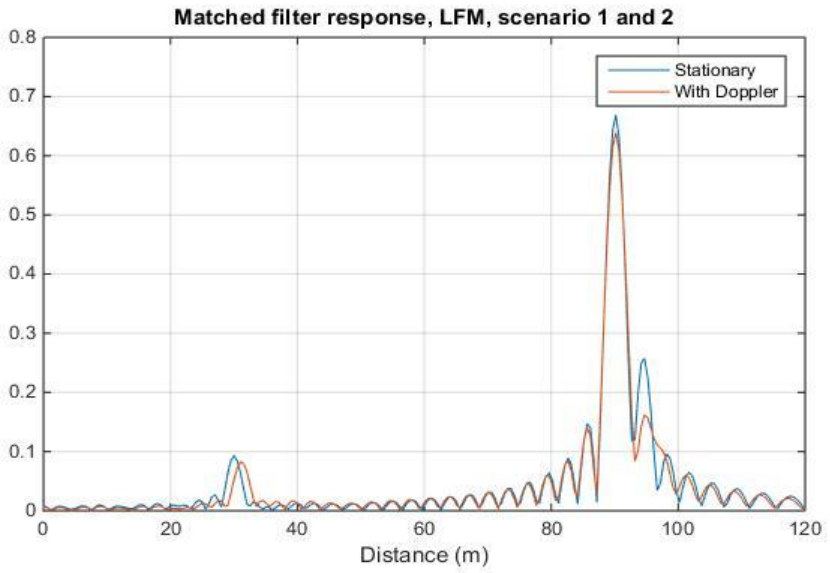

Figure 9 - Simulation results for targets illuminated with LFM pulse

In both scenarios, target 1 and 2 are clearly distinguishable. In scenario 1 (stationary targets), target 3, although close to target 2, still has a unique correlation peak and would likely result in detection. However, in scenario 2, both target 1 and 3 (the moving targets) show lower correlation peaks, as predicted by the ambiguity function for the LFM waveform. In fact, target 3 diminishes to the point where it is questionable whether or not target 3 would be classified as a unique target, since it lies within the sidelobe levels of target 2. Finally, the time delay of the Doppler shift (as predicted in the ambiguity plots) is seen in target 1 and target 3, and (falsely) shifts the position by about 2 meters.

The P4 simulation (shown in Figure 10) shows similar results to the LFM simulation for all targets for scenario 1. Target 3 stands out better than the LFM peak in the stationary scenario, owing to the low sidelobe level from target 2's sidelobes. However, in scenario 2, the echo of target 3 is now blended in with the mainlobe of target 2, with no distinct peak (as opposed to the LFM simulation, where target 3 still has a unique pulse, but with an amplitude comparable to the sidelobes of target 2). Furthermore, the mainlobes of all targets are attenuated. If this simulation had introduced a noise floor, the low-RCS targets could have possibly been attenuated below the noise floor. Clearly, Doppler shift has a more negative effect on the P4 waveform than the LFM waveform.

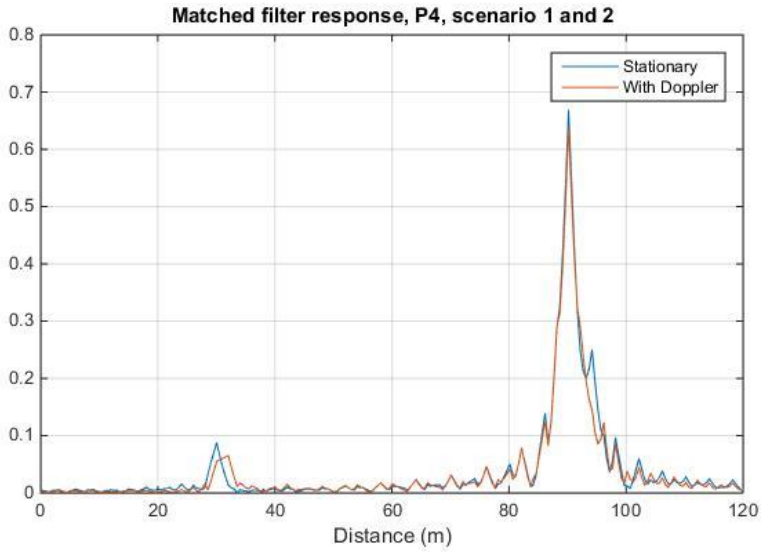

Figure 10 - Simulation results for targets illuminated with P4 pulse

Conclusions

The P4 waveform is considered a good waveform to use for military applications, in particular due to the low probability of intercept (LPIR) characteristics inherent in the waveform [8]. A very high bandwidth signal allows for lower transmit power (and hence detection by the enemy), and the pseudo-random nature of polyphase codes allows for blending in the signal with background noise and for system recognition. The very high velocities needed to see any negative effect on autocorrelation minimize any concern regarding the use of polyphase codes.
Ground penetrating radar is also a good application for polyphase codes. GPR doesn't require high transmit power (thus avoiding concerns about operating in the non-linear range of power amplifiers), can benefit from the low correlation sidelobes for sharper images, and has almost no Doppler shift to distort the autocorrelation.

In terms of practical use of polyphase codes, the high peak-to-average ratio, need for high-speed correlators, and transmission distortion through the power amplifiers are challenges that need to be addressed in order to efficiently use the waveforms while still preserving the good autocorrelation properties.

References

[1] IEEE Standard 686-2008, IEEE Standard Radar Definitions, May 2008.

[2] J.R. Klauder, A.C. Price, S. Darlington, and W.J. Albersheim, “The theory and design of chirp radars,” The Bell System Technical Journal, vol. XXXIX, no. 4, pp. 745-808, July 1960.

[3] Levanon, Nadav, Mozeson, Eli, *Radar Signals*, Wiley: Hoboken, NJ, 2004

[4] Blunt, Shannon D., Mokole, Eric L., An Overview of Radar Waveform Diversity, *IEEE Aerospace and Electronic Systems Magazine*, **31** 11 (Nov. 2016)

[5] Blunt, Shannon D., Cook, Matthew, Jakabosky, John, De Graaf, Jean, Perrins, Erik, Polyphase-Coded FM (PCFM) Radar Waveforms, Part I: Implementation, *IEEE Transactions on Aerospace and Electronic Systems*, **50**, 3 (July 2014) 2218-2227

[6] Anderson, Michael D., Resolution in Radar Mapping, Naval Postgraduate School, Mar. 1993.

[7] Yang, Jie, Sarkar, Tapan K., A novel Doppler-tolerant polyphase codes for pulse compression based on hyperbolic frequency modulation, *Digital Signal Processing* **17** (2007) 1019–1029

[8] Wehner, Donald R., *High Resolution Radar*, Artech House: Norward, MA, 1987

Appendix A – MATLAB CODE

```
% EECS725 Project - Ambiguity Plots
% This simulation will compare ambiguity functions of a linear frequency
% modulated (LFM), or "chirp", radar pulse transmission with a polyphase
% modulated P4 pulse for a pulse compression ratio of 64.

clear;
close all;

% Problem constraints
f_start   = 100e6;      % chirp start frequency (hz)
f_end     = 175e6;      % chirp end frequency (hz)
Nc        = 64;         % pulse compression ratio = BW * tau

% Simulation parameters
samp_per_chip = 3;      % (samples/chip)
f_max         = 25;     % Range of Doppler frequencies to plot (normalized to
f*tau)

% Derived parameters
bw        = f_end - f_start;        % bandwidth (hz)
t_b       = 1 / bw;                 % P4 chip period (s)
tau       = Nc / bw;                % pulse width (s)
t_samp    = t_b / samp_per_chip;    % simulation sampling period (s)
fd_max    = f_max / tau;            % Range of Doppler frequencies to plot
(hz)

t_burst   = linspace(0,tau,tau/t_samp)'; % vector of timestamps (s)

%% Chirp signal generation and analysis-------------------------------

% Generate chirp burst
k         = (f_end-f_start) / tau;          % chirp rate (hz/s)
theta_lfm = 2*pi*0.5*k.*(t_burst.^2);       % chirp phases
s_lfm_bb  = exp( j*theta_lfm );             % baseband chirp pulse

% Get autocorrelation of chirp
xc_lfm_bb = abs(xcorr(s_lfm_bb,'biased'));

% Construct ambiguity plot (LFM baseband)
amb_lfm_bb      = zeros((Nc*2)-1,100);
doppler_lag_idx = 1;
for f_shift=0:fd_max/99:fd_max
    s_lfm_bb_shifted = exp( -j*2*pi*f_shift.*t_burst ) .* s_lfm_bb;
    xc = abs(xcorr(s_lfm_bb,s_lfm_bb_shifted,'biased'));
    amb_lfm_bb(:,doppler_lag_idx) = xc(length(s_lfm_bb)-
Nc+1:length(s_lfm_bb)+Nc-1);
    doppler_lag_idx = doppler_lag_idx + 1;
end

%% P4 signal generation and analysis-----------------------------------

% Generate P4 chip sequence
```

```
theta_p4 = zeros(Nc,1);
for i=2:Nc
    theta_p4(i) = pi * ( (((i-1)^2)/Nc) - (i-1) ); % P4 phases
end

% Generate P4 signal (baseband)
s_p4_bb = zeros(length(t_burst),1);
for i=1:length(t_burst)
    s_p4_bb(i) = exp( j * theta_p4(mod(floor(i/samp_per_chip),Nc)+1) );
end

% Get autocorrelation of P4 (baseband)
xc_p4_bb = abs(xcorr(s_p4_bb,'biased'));

% Construct ambiguity plot (P4 baseband)
amb_p4_bb       = zeros((Nc*2)-1,100);
s_p4_bb_shifted = zeros(length(t_burst),1);
doppler_lag_idx = 1;
for f_shift=0:fd_max/99:fd_max
    s_p4_bb_shifted = exp( -j*2*pi*f_shift.*t_burst ) .* s_p4_bb;
    xc = abs(xcorr(s_p4_bb,s_p4_bb_shifted,'biased'));
    amb_p4_bb(:,doppler_lag_idx) = xc(length(s_p4_bb)-
Nc+1:length(s_p4_bb)+Nc-1);
    doppler_lag_idx = doppler_lag_idx + 1;
end

%% Plots-----------------------------------------------------------------

figure(1)
xa = linspace(0,f_max,100);
ya = linspace(-0.5/samp_per_chip,0.5/samp_per_chip,Nc*2-1);
surf(xa,ya,amb_p4_bb);
title('Ambuguity plot, P4 baseband');
ylabel('lag (t/\tau)');
xlabel('Doppler shift (f_d\tau)');
zlabel('\mid\chi(f_d,\tau)\mid');
grid on;

figure(2)
xa = linspace(0,f_max,100);
ya = linspace(-0.5/samp_per_chip,0.5/samp_per_chip,Nc*2-1);
surf(xa,ya,amb_lfm_bb);
title('Ambuguity plot, LFM baseband');
ylabel('lag (t/\tau)');
xlabel('Doppler shift (f_d\tau)');
zlabel('\mid\chi(f_d,\tau)\mid');
grid on;

figure(3)
stairs(theta_p4);
title('P4 sequence');
xlabel('Chip number');
ylabel('Phase (radians)');
grid on;
```

```
figure(4)
plot(20*log10(xc_lfm_bb));
hold on
plot(20*log10(xc_p4_bb));
title('ACS, LFM vs. P4')
xlabel('Lag');
ylabel('Power (dB)');
legend('LFM','P4');
grid on;
```

```
% EECS725 Project - Scenario simulation
% This simulation will compare performance of a linear frequency modulated
% (LFM), or "chirp", radar pulse transmission with a polyphase modulated P4
% transmission.

clear;
close all;

% Universal constants
c         = 3e8;       % speed of light (m/s)

% Problem constraints
f_start   = 10e9-(75e6/2); % chirp start frequency (hz)
f_end     = 10e9+(75e6/2); % chirp end frequency (hz)
Nc        = 128;           % pulse compression ratio = BW * tau

% Simulation parameters
samp_per_chip = 4;      % (samples/chip)
f_max         = 25;     % Range of Doppler frequencies to plot (normalized to
f*tau)

A_t1      = 0.1;        % amplitude of return, target 1
A_t2      = 1.0;        % amplitude of return, target 2
A_t3      = 0.25;       % amplitude of return, target 3
d_t1      = 30;         % target 1 distance (m)
d_t2      = 90;         % target 2 distance (m)
d_t3      = 94;         % target 3 distance (m)
s_t1      = 4412;       % speed, target 1 (m/s)
s_t2      = 0;          % speed, target 2 (m/s)
s_t3      = 4412;       % speed, target 3 (m/s)

% Derived parameters
bw        = f_end - f_start;        % bandwidth (hz)
t_b       = 1 / bw;                 % P4 chip period (s)
fc        = (f_start + f_end) / 2;  % center (carrier) frequency for P4 (hz)
tau       = Nc / bw;                % pulse width (s)
t_samp    = t_b / samp_per_chip;    % simulation sampling period (s)
fd_max    = f_max / tau;            % Range of Doppler frequencies to plot
(hz)
fd_t1     = 2 * fc * s_t1 / c;      % Doppler shift (hz), target 1
fd_t2     = 2 * fc * s_t2 / c;      % Doppler shift (hz), target 2
fd_t3     = 2 * fc * s_t3 / c;      % Doppler shift (hz), target 3

i_t1      = floor(2*d_t1/(c*t_samp));     % index of first target
i_t2      = floor(2*d_t2/(c*t_samp));     % index of second target
i_t3      = floor(2*d_t3/(c*t_samp));     % index of third target
t_burst   = linspace(0,tau,tau/t_samp)'; % vector of timestamps (s)

% Printout system parameters
fprintf(1,'Bandwidth = %5.2d Mhz\n',bw/1e6);
fprintf(1,'Pulse duration = %5.2d us\n',tau*1e6);
fprintf(1,'Range resolution = %5.2d m\n',c/(2*bw));
fprintf(1,'Simulation sampling frequency = %5.2d Mhz\n',1/(1e6*t_samp));
```

```
%% Chirp signal generation and analysis---------------------------------

% Generate chirp burst
k         = (f_end-f_start) / tau;           % chirp rate (hz/s)
theta_lfm = 2*pi*0.5*k.*(t_burst.^2);        % chirp phases
s_lfm     = cos( 2*pi*(f_start.*t_burst + 0.5*k.*(t_burst.^2)) );
s_lfm_bb  = exp( j*theta_lfm );              % baseband chirp pulse

% Get passband PSD of chirp
[Pss_lfm,w] = periodogram(s_lfm,[],1024);
f_plot  = w / (2*pi*t_samp);

% Get autocorrelation of chirp
xc_lfm_bb = abs(xcorr(s_lfm_bb,'biased'));

% Construct ambiguity plot (LFM baseband)
amb_lfm_bb      = zeros((Nc*2)-1,100);
doppler_lag_idx = 1;
for f_shift=0:fd_max/99:fd_max
    s_lfm_bb_shifted = exp( -j*2*pi*f_shift.*t_burst ) .* s_lfm_bb;
    xc = abs(xcorr(s_lfm_bb,s_lfm_bb_shifted,'biased'));
    amb_lfm_bb(:,doppler_lag_idx) = xc(length(s_lfm_bb)-
Nc+1:length(s_lfm_bb)+Nc-1);
    doppler_lag_idx = doppler_lag_idx + 1;
end

%% P4 signal generation and analysis-----------------------------------

% Generate P4 chip sequence
theta_p4 = zeros(Nc,1);
for i=2:Nc
    theta_p4(i) = pi * ( (((i-1)^2)/Nc) - (i-1) ); % P4 phases
end

% Generate P4 signal (baseband and passband signal)
s_p4_bb = zeros(length(t_burst),1);
for i=1:length(t_burst)
    s_p4_bb(i) = exp( j * theta_p4(mod(floor(i/samp_per_chip),Nc)+1) );
end
s_p4 = real( s_p4_bb .* exp(j*2*pi*fc.*t_burst) );

% Get passband PSD of P4 signal
[Pss_P4,w_P4] = periodogram(s_p4,[],1024);
f_plot_P4     = w_P4 / (2*pi*t_samp);

% Get autocorrelation of P4 (baseband)
xc_p4_bb = abs(xcorr(s_p4_bb,'biased'));

% Construct ambiguity plot (P4 baseband)
amb_p4_bb       = zeros((Nc*2)-1,100);
s_p4_bb_shifted = zeros(length(t_burst),1);
doppler_lag_idx = 1;
for f_shift=0:fd_max/99:fd_max
    s_p4_bb_shifted = exp( -j*2*pi*f_shift.*t_burst ) .* s_p4_bb;
    xc = abs(xcorr(s_p4_bb,s_p4_bb_shifted,'biased'));
```

```
    amb_p4_bb(:,doppler_lag_idx) = xc(length(s_p4_bb)-
Nc+1:length(s_p4_bb)+Nc-1);
    doppler_lag_idx = doppler_lag_idx + 1;
end

%% Simulation start-----------------------------------------------------

% Generate composite radar return signal (LFM), scenario 1
s_lfm_bb_tx = s_lfm_bb;
r = zeros(2*length(s_lfm_bb_tx),1);
r_t1 = r;
r_t2 = r;
r_t3 = r;
r_t1(i_t1:length(s_lfm_bb_tx)+i_t1-1) = A_t1 * s_lfm_bb_tx;
r_t2(i_t2:length(s_lfm_bb_tx)+i_t2-1) = A_t2 * s_lfm_bb_tx;
r_t3(i_t3:length(s_lfm_bb_tx)+i_t3-1) = A_t3 * s_lfm_bb_tx;
r = r_t1 + r_t2 + r_t3;

% Cross-correlate transmit and receive signals
xc_out_lfm  =
flipud(abs(xcorr(s_lfm_bb_tx,r(1:length(s_lfm_bb_tx)),'biased')));
mixer_out_lfm_1 = xc_out_lfm(floor(length(xc_out_lfm)/2):length(xc_out_lfm));

% Generate composite radar return signal (LFM), scenario 2
r = zeros(2*length(s_lfm_bb_tx),1);
r_t1 = r;
r_t2 = r;
r_t3 = r;
r_t1(i_t1:length(s_lfm_bb_tx)+i_t1-1) = A_t1 * s_lfm_bb_tx .* exp( -
j*2*pi*fd_t1.*t_burst );
r_t2(i_t2:length(s_lfm_bb_tx)+i_t2-1) = A_t2 * s_lfm_bb_tx .* exp( -
j*2*pi*fd_t2.*t_burst );
r_t3(i_t3:length(s_lfm_bb_tx)+i_t3-1) = A_t3 * s_lfm_bb_tx .* exp( -
j*2*pi*fd_t3.*t_burst );
r = r_t1 + r_t2 + r_t3;

% Cross-correlate transmit and receive signals
xc_out_lfm  =
flipud(abs(xcorr(s_lfm_bb_tx,r(1:length(s_lfm_bb_tx)),'biased')));
mixer_out_lfm_2 = xc_out_lfm(floor(length(xc_out_lfm)/2):length(xc_out_lfm));

% Generate composite radar return signal (P4), scenario 1
s_p4_bb_tx = s_p4_bb;
r = zeros(2*length(s_p4_bb_tx),1);
r_t1 = r;
r_t2 = r;
r_t3 = r;
r_t1(i_t1:length(s_p4_bb_tx)+i_t1-1) = A_t1 * s_p4_bb_tx;
r_t2(i_t2:length(s_p4_bb_tx)+i_t2-1) = A_t2 * s_p4_bb_tx;
r_t3(i_t3:length(s_p4_bb_tx)+i_t3-1) = A_t3 * s_p4_bb_tx;
r = r_t1 + r_t2 + r_t3;

% Cross-correlate transmit and receive signals
xc_out_p4  = flipud(abs(xcorr(s_p4_bb_tx,r(1:length(s_p4_bb_tx)),'biased')));
mixer_out_p4_1 = xc_out_p4(floor(length(xc_out_p4)/2):length(xc_out_p4));
```

```
% Generate composite radar return signal (P4), scenario 2
r = zeros(2*length(s_p4_bb_tx),1);
r_t1 = r;
r_t2 = r;
r_t3 = r;
r_t1(i_t1:length(s_p4_bb_tx)+i_t1-1) = A_t1 * s_p4_bb_tx .* exp( -
j*2*pi*fd_t1.*t_burst );
r_t2(i_t2:length(s_p4_bb_tx)+i_t2-1) = A_t2 * s_p4_bb_tx .* exp( -
j*2*pi*fd_t2.*t_burst );
r_t3(i_t3:length(s_p4_bb_tx)+i_t3-1) = A_t3 * s_p4_bb_tx .* exp( -
j*2*pi*fd_t3.*t_burst );
r = r_t1 + r_t2 + r_t3;

% Cross-correlate transmit and receive signals
xc_out_p4  = flipud(abs(xcorr(s_p4_bb_tx,r(1:length(s_p4_bb_tx)),'biased')));
mixer_out_p4_2 = xc_out_p4(floor(length(xc_out_p4)/2):length(xc_out_p4));

%% Plots------------------------------------------------------------

figure(1)
plot(linspace(0,length(mixer_out_p4_1)*c*t_samp/2,length(mixer_out_p4_1)),abs
(mixer_out_p4_1));
hold on;
plot(linspace(0,length(mixer_out_p4_2)*c*t_samp/2,length(mixer_out_p4_1)),abs
(mixer_out_p4_2));
grid on;
title('Matched filter response, P4, scenario 1 and 2');
xlabel('Distance (m)');
legend('Stationary','With Doppler');
axis([0 120 0 0.8]);


figure(2)
plot(linspace(0,length(mixer_out_lfm_1)*c*t_samp/2,length(mixer_out_lfm_1)),a
bs(mixer_out_lfm_1));
hold on;
plot(linspace(0,length(mixer_out_lfm_2)*c*t_samp/2,length(mixer_out_lfm_2)),a
bs(mixer_out_lfm_2));
grid on;
title('Matched filter response, LFM, scenario 1 and 2');
xlabel('Distance (m)');
legend('Stationary','With Doppler');
axis([0 120 0 0.8]);

figure(3)
xa = linspace(0,f_max,100);
ya = linspace(-0.5/samp_per_chip,0.5/samp_per_chip,Nc*2-1);
surf(xa,ya,amb_p4_bb);
title('Ambuguity plot, P4 baseband');
ylabel('lag (t/\tau)');
xlabel('Doppler shift (f_d\tau)');
grid on;
```

```
figure(4)
xa = linspace(0,f_max,100);
ya = linspace(-0.5/samp_per_chip,0.5/samp_per_chip,Nc*2-1);
surf(xa,ya,amb_lfm_bb);
title('Ambuguity plot, LFM baseband');
ylabel('lag (t/\tau)');
xlabel('Doppler shift (f_d\tau)');
grid on;

figure(5)
plot(20*log10(xc_lfm_bb));
hold on
plot(20*log10(xc_p4_bb));
title('ACS, LFM vs. P4')
xlabel('Lag');
ylabel('Power (dB)');
legend('LFM','P4');
grid on;

figure(6)
plot(f_plot_P4,20*log10(Pss_P4));
hold on
plot(f_plot,20*log10(Pss_lfm));
title('PSD of LFM and P4, Fc=200Mhz, BW=75Mhz');
xlabel('Frequency (hz)');
ylabel('Power (dB)');
legend('P4','LFM');
grid on;
```